Heparin-dependent aggregation of hen egg white lysozyme reveals two distinct mechanisms of amyloid fibrillation

Received for publication, August 17, 2017, and in revised form, October 19, 2017 Published, Papers in Press, November 3, 2017, DOI 10.1074/jbc.M117.813097

Ayame Nitani[‡1], Hiroya Muta[‡1], Masayuki Adachi[‡1], Masatomo So[‡], Kenji Sasahara[‡], Kazumasa Sakurai[§], Eri Chatani[¶], Kazumitsu Naoe[‖], Hirotsugu Ogi[**], Damien Hall[‡ ‡‡2], and Yuji Goto[‡3]

From the [‡]Institute for Protein Research, Osaka University, Yamadaoka 3-2, Suita, Osaka 565-0871, Japan, [§]Institute of Advanced Technology, Kindai University, 930 Nishimitani, Kinokawa, Wakayama 649-6493, Japan, [¶]Department of Chemistry, Graduate School of Science, Kobe University, Hyogo 657-8501, Japan, [‖]National Institute of Technology, Nara College, Nara 639-1080, Japan, [**]Graduate School of Engineering, Suita, Osaka 565-0871, Japan, and [‡‡]Research School of Chemistry, Australian National University, Acton, ACT 2601, Australia

Edited by Paul E. Fraser

Heparin, a biopolymer possessing high negative charge density, is known to accelerate amyloid fibrillation by various proteins. Using hen egg white lysozyme, we studied the effects of heparin on protein aggregation at low pH, raised temperature, and applied ultrasonic irradiation, conditions under which amyloid fibrillation was promoted. Heparin exhibited complex bimodal concentration-dependent effects, either accelerating or inhibiting fibrillation at pH 2.0 and 60 °C. At concentrations lower than 20 μg/ml, heparin accelerated fibrillation through transient formation of hetero-oligomeric aggregates. Between 0.1 and 10 mg/ml, heparin rapidly induced amorphous hetero-aggregation with little to no accompanying fibril formation. Above 10 mg/ml, heparin again induced fibrillation after a long lag time preceded by oligomeric aggregate formation. Compared with studies performed using monovalent and divalent anions, the results suggest two distinct mechanisms of heparin-induced fibrillation. At low heparin concentrations, initial hen egg white lysozyme cluster formation and subsequent fibrillation is promoted by counter ion binding and screening of repulsive charges. At high heparin concentrations, fibrillation is caused by a combination of salting out and macromolecular crowding effects probably independent of protein net charge. Both fibrillation mechanisms compete against amorphous aggregation, producing a complex heparin concentration–dependent phase diagram. Moreover, the results suggest an active role for amorphous oligomeric aggregates in triggering fibrillation, whereby breakdown of supersaturation takes place through heterogeneous nucleation of amyloid on amorphous aggregates.

The formation of amyloid, a type of fibrillar protein aggregate associated with the etiology of ~50 disease states (1–3), is enigmatic because of the fact that it involves the ordered linear assembly of a disordered structural state. As such, gaining an understanding of the mechanism of amyloid fibrillation is important both for advancing protein science and preventing human disease. Since the development of the infectious amyloid/prion concept, positive comparisons between the processes of amyloid fibrillation and molecular crystallization have been noted (4–7). These similarities include the following: cooperative reaction kinetics after a lag time, distinct morphologies of the fibril/crystal structure depending on the conditions, and the seed-dependent propagation of unique fibril/crystal structural morphology (4–7). Such underlying commonalities suggest that, as for the case of crystallization, amyloid fibrillation is a supersaturation-limited precipitation of denatured proteins, which occurs only above solubility (*i.e.* critical concentration) (8). We recently reviewed evidence indicating the role of supersaturation in determining amyloid fibrillation (9) and suggested how this classical viewpoint, adapted from the molecular crystallization literature, may complement structural studies in further advancing understanding of protein aggregation (8–11).

In general, there are two types of solid state structure that a solute may adopt above solubility. One is crystalline, which involves organized and repetitive arrangement of the molecules, whereas the other is amorphous (glasslike), in which the solid is formed without appreciable internal ordering of the solute (8–11). It is often assumed that the amorphous aggregate designation accommodates oligomers responsible for cytotoxicity of amyloidogenic proteins (12, 13). However, despite their potential medical importance, the role that amorphous aggregates play in amyloid fibrillation is far from clear. From the viewpoint of crystallography, although crystals form at solute concentrations above the critical concentration, amorphous glasses may have their own solubility, thereby distorting the

This work was performed under the Cooperative Research Program for the Institute for Protein, Osaka University, ICR-15-02, CR-16-02, and VFCR-16-04 and was supported by JSPS KAKENHI Grants 15H04362, 15K14458, 15K07038, 16H00836, 17K07363, and 17H06352 and by the SENTAN from Japan Agency for Medical Research and Development (AMED). The authors declare that they have no conflicts of interest with the contents of this article.

This article contains Supporting Methods, Supporting Results, Figs. S1–S10, and Table S1.

[1] These authors contributed equally to this work.

[2] Recipient of a Senior Research Fellowship from the Australian National University and a Cross-Appointment Fellowship from the Institute for Protein Research.

[3] To whom correspondence should be addressed. E-mail: gtyj8126@protein.osaka-u.ac.jp.

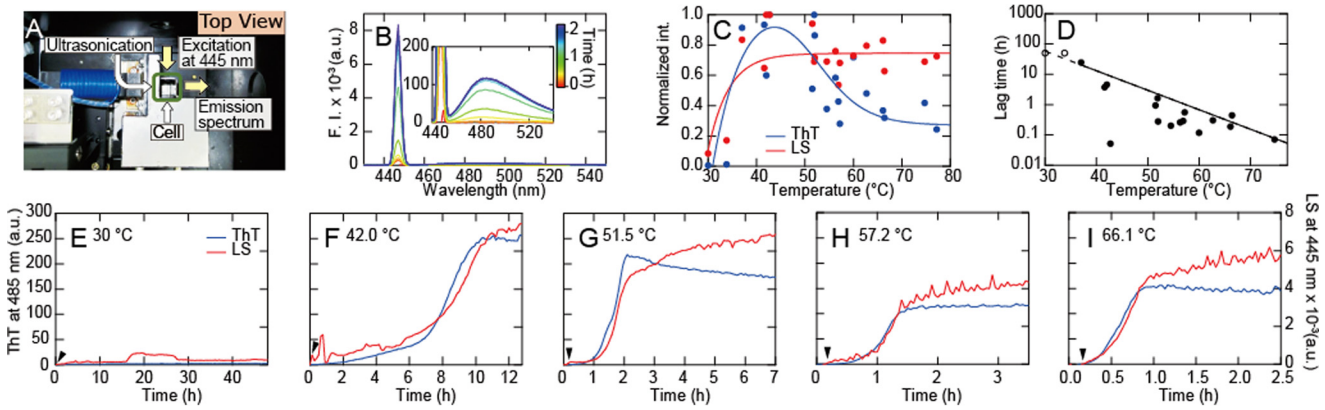

Figure 1. Fibril formation of HEWL and its temperature dependence. Fibrillation of HEWL at 0.25 mg/ml in 100 mM NaCl, 10 mM HCl (pH 2.0) at various temperatures was monitored by fluorometer with ultrasonicator attached to a cell. *A*, experimental setup for irradiation of the solution with ultrasonic pulses and simultaneous monitoring of light scattering and ThT fluorescence (see Ref. 8). *B*, repeated measurements of spectra at 60 °C. *C* and *D*, temperature dependence of the light scattering at 445 nm and ThT fluorescence (*C*) and lag time (*D*). *E–I*, kinetics of fibrillation at various temperatures monitored by light scattering at 445 nm (*red*) and ThT fluorescence at 485 nm (*blue*) with excitation at 445 nm. HEWL was added at 10 min after the start of recording and is indicated by *arrowhead*.

kinetic and thermodynamic relations governing crystal formation in the absence of this alternative aggregation pathway (13, 14). By analyzing the salt-dependent fibrillation and amorphous aggregation of β_2-microglobulin (β2m),[4] the protein responsible for dialysis-related amyloidosis, we proposed that amyloid fibrils and amorphous aggregates correspond to crystals and glasses of solutes, respectively (8, 9). We also proposed that amorphous aggregate formation, when occurring in competition with fibrillation, represents a trapped state, which might be later converted to fibrils (14, 15). Although nonseeded amyloid fibrillation typically occurs slowly, via a homogeneous nucleation pathway defined by a long lag time/high free–energy nucleation barrier (10), amorphous aggregation generally occurs rapidly, absent any such nucleation barrier (8). This relative "speed out of the gates" can mean that the kinetics of amorphous aggregate formation/dissolution may effectively define the apparent kinetic and thermodynamic behavior of the denatured monomer/amyloid phase transition via its participation as a competitive pathway (13–15).

Another parallel from the molecular crystallization literature that may be drawn upon when discussing the mechanism of fibrillation is the role of ternary components in facilitating crystallization and/or breakage of supersaturated solution conditions (with solvent and solute representing a binary system). In this regard, the effects of various inhibitors or accelerators of amyloid formation have been examined, with the twin aims of developing therapeutic strategies and understanding the mechanism of fibrillation (16–21). Although various salts or detergents are known to promote fibrillation, above certain concentrations they may prevent fibrillation by inducing amorphous aggregation. Such concentration-dependent promotion and inhibition produces a bell-shaped profile, able to be understood on the basis of traditional phase diagrams of crystallization accommodating both crystals and glasses (8, 22).

[4] The abbreviations used are: β2m, β_2-microglobulin; Gdn-HCl, guanidine hydrochloride; HEWL, hen egg white lysozyme; ThT, thioflavin T; TEM, transmission electron microscopy; TFE, trifluoroethanol.

Among the plethora of studied additives, the biopolymer heparin, a long unbranched chain polysaccharide possessing a large number of sulfate groups (*i.e.* one to three sulfate groups per disaccharide unit with "one" negative charge per sulfate group), has been studied extensively because of its biological relevance (16–20, 23–27). Heparin is one of the most common glycosaminoglycans found in our body and is often used to prevent blood coagulation in patients taking hemodialysis. Heparin is known to exhibit complicated effects on amyloid fibrillation dependent on the protein and solvent condition (18–20). We have previously shown that heparin also exhibits a bell-shaped acceleration and inhibition profile on the fibrillation of β2m (27). However, the exact details of the mechanism of acceleration and inhibition have, until this present study, remained unknown. Using hen egg white lysozyme (HEWL), we first demonstrate that the complex pattern of heparin-induced acceleration and inhibition of HEWL fibrillation can be explained (to first order) by a competition between fibrillation and amorphous aggregation. We then demonstrate that there are two types of processes (*i.e.* counter–ion binding and general salting out/macromolecular crowding) by which heparin acts to induce aggregation. We further refine the model by suggesting a second-order effect in which fibrillation may be triggered by a small amount of template-competent amorphous aggregates accumulated under supersaturation.

Results

Ultrasonication-forced fibrillation of HEWL and its temperature dependence

To both accelerate and directly monitor fibrillation of HEWL, we used a self-constructed spectrofluorometer with ultrasonicator attached to the cell (Fig. 1*A*, see also Fig. S1 of Ref. 8). Through intermittent measurement of thioflavin T (ThT) fluorescence at 485 nm and 90° light scattering at 445 nm, we simultaneously monitored signals reflecting fibrillation and total aggregate formation (28). At pH 2.0 (10 mM HCl) and 0.1 M NaCl, fibrillation was accelerated upon increasing temperature from 30 to 70 °C. The enhancement in rate with tem-

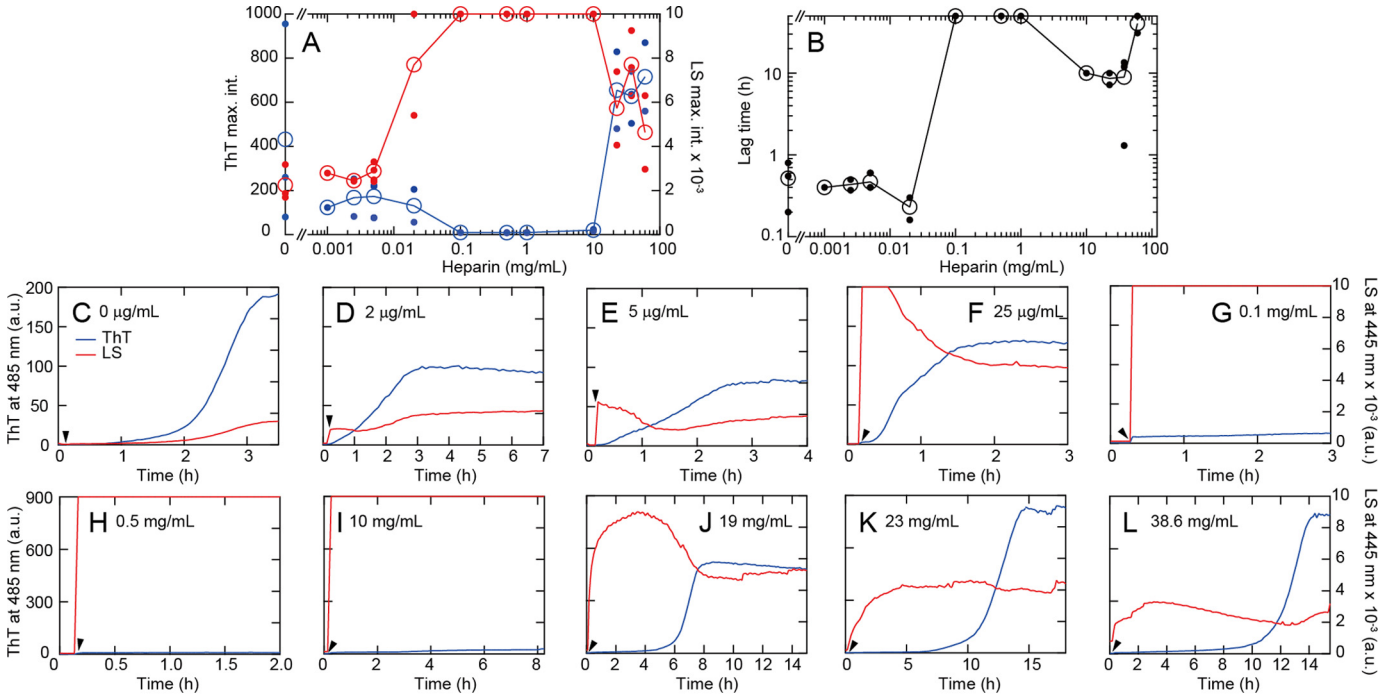

Figure 2. HEWL fibrillation in the presence of various concentrations of heparin at 0.1 M NaCl and 60 °C. *A* and *B*, dependence of maximal ThT fluorescence (*blue line*) and light scattering (*red line*) intensities (*A*) and lag time (*B*) on heparin concentration. *Open symbols* indicate the average values and *small closed symbols* indicate the observed data; when only one data point was available, they are overlapped. The same is true for Fig. 5. *C–L*, kinetics of aggregation monitored by light scattering at 445 nm (*red*) and ThT fluorescence at 485 nm (*blue*) at various heparin concentrations. HEWL was added at 10 min after the start of recording and is indicated by a *solid arrowhead*.

perature was such that no fibrillation was observed over 3 days at 30 °C whereas the fibrillation reaction was essentially completed after 1 h at 70 °C (recorded lag time of 10 min). The observed temperature-dependent acceleration was linked to the fractional extent of HEWL thermal unfolding for which the midpoint unfolding temperature, T_m, was measured to be 57 °C in 10 mM HCl (Fig. S1*A*). For the aggregation of HEWL solutions possessing no additional macromolecular components, the kinetics of fibrillation monitored by ThT fluorescence was essentially coincidental with that monitored by light scattering, suggesting that fibrillation occurred without significant accumulation of amorphous aggregates or oligomers (28, 29).

Fibrillation at various concentrations of heparin at 60 °C

The effects of heparin on HEWL fibrillation were examined at 60 °C, 10 mM HCl (pH 2.0), 0.1 M NaCl, and heparin concentrations ranging from several μg/ml to 60 mg/ml. Heparin exhibited complex concentration-dependent effects either accelerating or inhibiting fibrillation (Fig. 2). In the absence of heparin, fibrillation occurred with a lag time of ~0.8 h. In the presence of concentrations of heparin up to a few μg/ml, a slight promotion in fibrillation rate was observed as evidenced by a decrease in lag time of ThT fluorescence (*blue line*). This low concentration of heparin also induced an immediate and slight increase in light scattering at 445 nm. Light-scattering decrease was accompanied by a subsequent increase in ThT fluorescence. Addition of heparin concentrations above 0.1 mg/ml resulted in rapid and significant increases in light scattering within the 10-s dead time of the measurement. Notably, the immediate development of light scattering was not followed by a production of ThT fluorescence. For all cases above 0.1 mg/ml heparin concentration the solution was visibly turbid.

Interestingly, the extent of total aggregation, as measured by light scattering at 445 nm, decreased above 19 mg/ml of added heparin. As scattering is a property reflecting the difference in polarizability of the scattering component to the surrounding medium, the observed decrease may be because of changes in the bulk refractive index of the solution or it may be because of a reduction in aggregate size and/or shape or extent (28). An increase in ThT fluorescence was again observed at 19 mg/ml heparin (Fig. 2*J*). After a long lag period of 6 h, ThT fluorescence increased cooperatively to a value several times higher than those at lower heparin concentrations. At even higher heparin concentrations of 23 or 39 mg/ml, the lag time was markedly longer (Fig. 2, *K* and *L*). Thermal unfolding of HEWL monitored by circular dichroism (CD) spectroscopy showed that high heparin concentrations stabilized the native state (Fig. S1*Q*). This increased stability of the native state coupled with oligomer formation likely retards fibrillation in the presence of high concentrations of heparin (see below).

Solutions with increased ThT fluorescence (in the presence or absence of heparin) showed CD spectra typical for β-sheet containing amyloid fibrils (Fig. 3*D*), in contrast to the CD spectrum of native HEWL which revealed the expected mixture of α-helical and β-sheet content (Fig. 3*B*). Transmission electron microscopy (TEM) images showed that solutions exhibiting ThT fluorescence contained protein aggregates with rodlike morphology typical for amyloid fibrils (Fig. 3*A*). Although the marked ThT fluorescence intensity of fibrils formed at high heparin concentrations suggests distinct fibril structures from

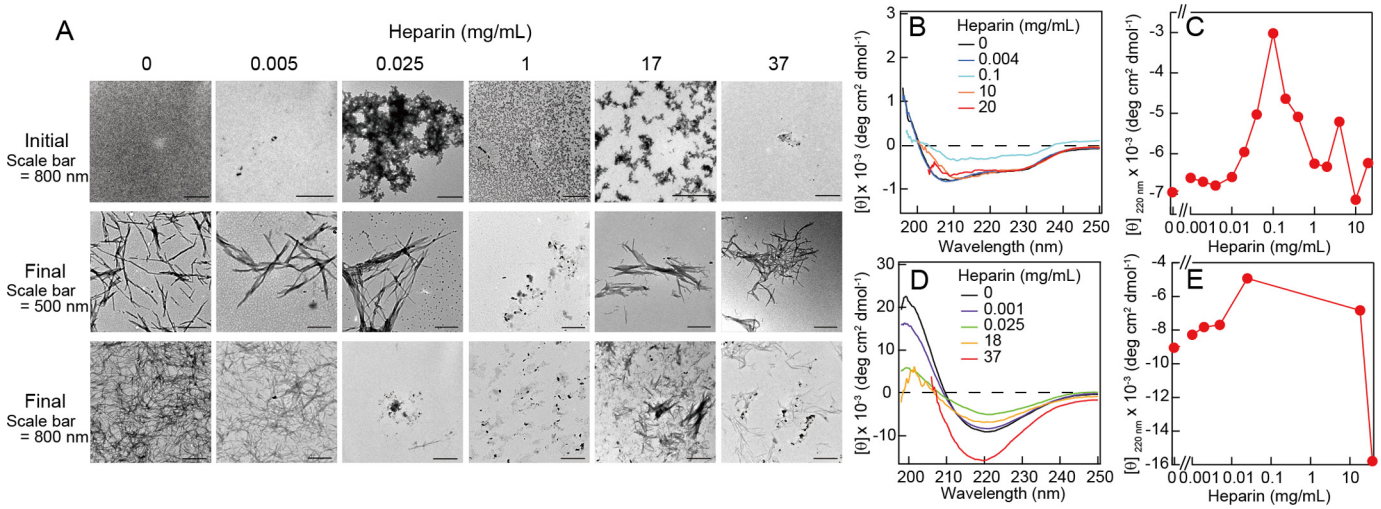

Figure 3. Morphologies and conformations of HEWL fibrils formed in the presence of various concentrations of heparin. *A*, TEM images obtained before and after ultrasonic treatments. *B–E*, CD spectra were obtained before (*B*) and after (*D*) ultrasonic treatments. Dependence of the ellipticity at 220 nm on heparin concentration are shown (*C* and *E*).

those formed at low heparin concentrations, details are unknown at this stage. It should be noted that that different types of amyloid conformations, which could be formed under distinct heparin concentration regimes, would show different ThT intensities. In contrast, we confirmed significant formation of amorphous aggregates at intermediate concentrations of heparin by TEM imaging (both at the initial and final phases of the aggregation time course) (Fig. 3*A*).

To examine the affinity of heparin and HEWL, we performed a series of isothermal titration calorimetry (ITC) measurements in 10 mM HCl (pH 2.0) at 37 °C (Fig. S2). The exothermic heat below ~10 mg/ml heparin indicated that strong electrostatic interactions between the negatively charged heparin and positively charged HEWL molecules underlie the heparin-dependent amyloid formation and amorphous aggregation. On the other hand, a smaller exothermic heat above 10 mg/ml heparin suggested that the heparin-dependent amyloid formation at very high concentrations of heparin might be caused by a mechanism distinct from the charge-charge interactions.

Distinguishing amorphous aggregates and amyloid fibrils by direct imaging

To readily distinguish between amyloid fibrils and amorphous aggregates, we compared photographic images of the solutions in wells of a microplate illuminated using either white incident light or LED light at 440 nm (Fig. 4 and Fig. S3). In this experiment, ultrasonicated samples containing 5 μM ThT were transferred from the custom fluorometer setup to the wells of a microplate. Turbid well images generated under white light were taken as indicating total aggregation (amorphous and amyloid), although fibrils tended to exhibit green-yellow color with less turbidity. Blue fluorescent images obtained under 440 nm light were taken as specifically indicating fibrils. With this direct technique, experiments were performed using HEWL solutions supplemented with various concentrations of heparin and incubated overnight under quiescent conditions.

These studies showed that only amorphous aggregates were formed at 37 or 60 °C between 0.02 and 22.5 mg/ml heparin. Upon ultrasonication at 60 °C, fibrils formed at low (<5 μg/ml) heparin concentrations, in agreement with the results obtained with the single cuvette fluorometer. In the intervening heparin concentration range (0.02–10 mg/ml) amorphous aggregates remained even under ultrasonication. Fibrils with marked ThT fluorescence again became dominant above 22.5 mg/ml heparin. Such direct photographic images clearly show that the amyloid fibrils and amorphous aggregates are promoted under different regimes of the solution phase space and that their populations are inversely related to each other over the range of heparin concentrations studied.

Low-temperature trapping and high temperature–induced fibrillation

To investigate the mechanism of the low concentration heparin-dependent promotion of amyloid fibrillation observed at 60 °C, we systematically monitored the aggregation reaction at a series of low temperatures (Fig. S4, *A* and *B*). At 5 °C in the presence of 5 μg/ml heparin, a slight increase in light scattering still occurred within the dead time of measurement with no concomitant change in ThT fluorescence. Incubation of the solution at 5 °C for a 10-h period with subsequent sequential increases in temperature to 25 and 37 °C did not significantly change the light scattering and ThT signals (as also indicated by the small changes in extent of temperature-dependent oligomerization monitored by dynamic light scattering and analytical ultracentrifugation at these low temperatures, Figs. S5 and S6). However, an increase in temperature to 60 °C was accompanied by a sudden increase in both ThT fluorescence and light scattering. In interpreting this result, we note that at lower temperatures two factors are operative. The first relates to protein stability *i.e.* the protein adopts a more stable structure below its T_m value (Fig. S1). The second pertinent factor is that heparin association with HEWL will likely result in trapped HEWL conformations. To explain the apparent trapping of HEWL at lower temperatures, we postulated that the sudden rise in temperature both promoted a more concentrated and labile HEWL by dissociation from a hetero-oligomeric cluster (*i.e.* faster

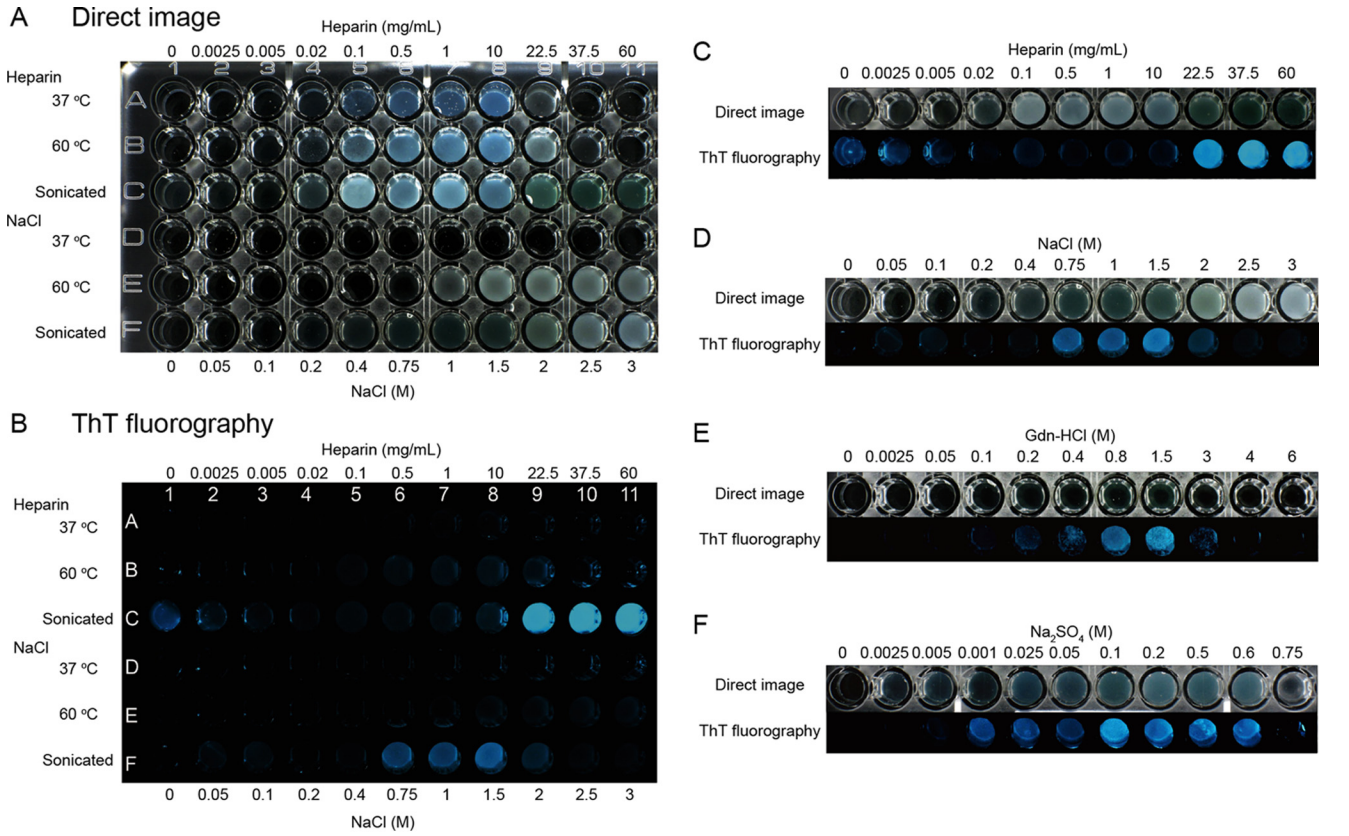

Figure 4. Distinguishing amorphous aggregates and amyloid fibrils by direct imaging. *A* and *B*, direct turbidimetric (*A*) and ThT fluorescence (*B*) photographic images were observed under illumination of white light and LED 445 nm light, respectively. *C–F*, direct and ThT fluorescence images for the rows at 60 °C after ultrasonic treatment are compared. Dependences on heparin (*C*) and NaCl (*D*) were made from plate images (*A*) and (*B*). Those on Gdn-HCl (*E*) and Na_2SO_4 (*F*) were made from plate images of Fig. S2. All the solutions contained 0.2 mg/ml HEWL, 5 μM ThT, and 10 mM HCl (pH 2.0). Ultrasonicated samples were taken after the measurements with a fluorometer as shown in Fig. 2. Other samples without ultrasonication were prepared and incubated overnight at 37 or 60 °C.

dynamics) as well as producing a more denatured HEWL, with these two factors jointly enhancing fibrillation. The kinetics of heat-induced conversion to fibrils (Fig. S4, *A* and *B*) were similar to the kinetics observed at 60 °C without incubation at lower temperatures (Fig. 2*E*), indicating that production of oligomeric species, even if accumulated at lower temperature, was not rate-limiting with regard to the fibrillation reaction. A similar low-temperature trapping behavior of native oligomers and high-temperature conversion to amyloid fibrils was observed at high heparin concentrations (*i.e.* 19 and 38 mg/ml) (Fig. S4, *C* and *D*).

Fibrillation in the presence of heparin under milder conditions

To investigate the effects of heparin at ambient temperature, we used the HANABI device (developed in our laboratory) which combines ultrasonication with a 96-well microplate fluorometer (Fig. S7) (30). We chose conditions of 10 mM HCl, 0.5 M Gdn-HCl, and 37 °C, for which, in the absence of heparin, no fibrillation occurred for at least 2 days (*i.e.* the lag time of fibrillation was longer than 50 h) because of stabilization of the native state (30). At 0.05 mg/ml of added heparin, fibrillation was notably accelerated with an average lag time of 10 h. Further increases in heparin concentration decreased the final ThT fluorescence and increased the lag time. Above 25 mg/ml heparin, no significant increase in ThT fluorescence was detected, *i.e.* the second stage of fibrillation observed above 20 mg/ml at 60 °C under ultrasonication (Fig. 2) was not seen, the reason for the lack of this second stage possibly because of the greater stability of the HEWL native state at 37 °C (Fig. S1).

Seeding reactions

We examined the kinetics of seeded aggregation reactions at 60 °C in the absence and presence of 20 mg/ml of heparin with seed fibrils formed under the same solution conditions (Fig. S4, *E–H*). In the absence of heparin at 0.1 M NaCl and 60 °C, the lag phase disappeared upon seeding, a finding completely consistent with a seed-dependent elongation mechanism (7). Although the lag time was effectively halved (6 h to 3 h) in the presence of 19 mg/ml heparin, the fact that the lag phase remained indicated that release of the HEWL monomer from the trapped hetero-oligomeric state may be rate-limiting.

Fibrillation in the presence of various salts

To more fully understand the complex effects of heparin on the fibrillation of HEWL, we examined the effects of various salts (NaCl, Gdn-HCl, and Na_2SO_4) on the fibrillation reaction at 60 °C in 10 mM HCl with ultrasonication (Fig. 5 and Fig. S8). Concentrations ranging from 0.05 to 1.0 M NaCl induced fibrillation with some amorphous aggregate evident at 0.2 M. Above 1.5 M NaCl, fibrillation was suppressed and amorphous aggregation became dominant (as revealed by an increase in light scattering and a decrease in ThT fluorescence).

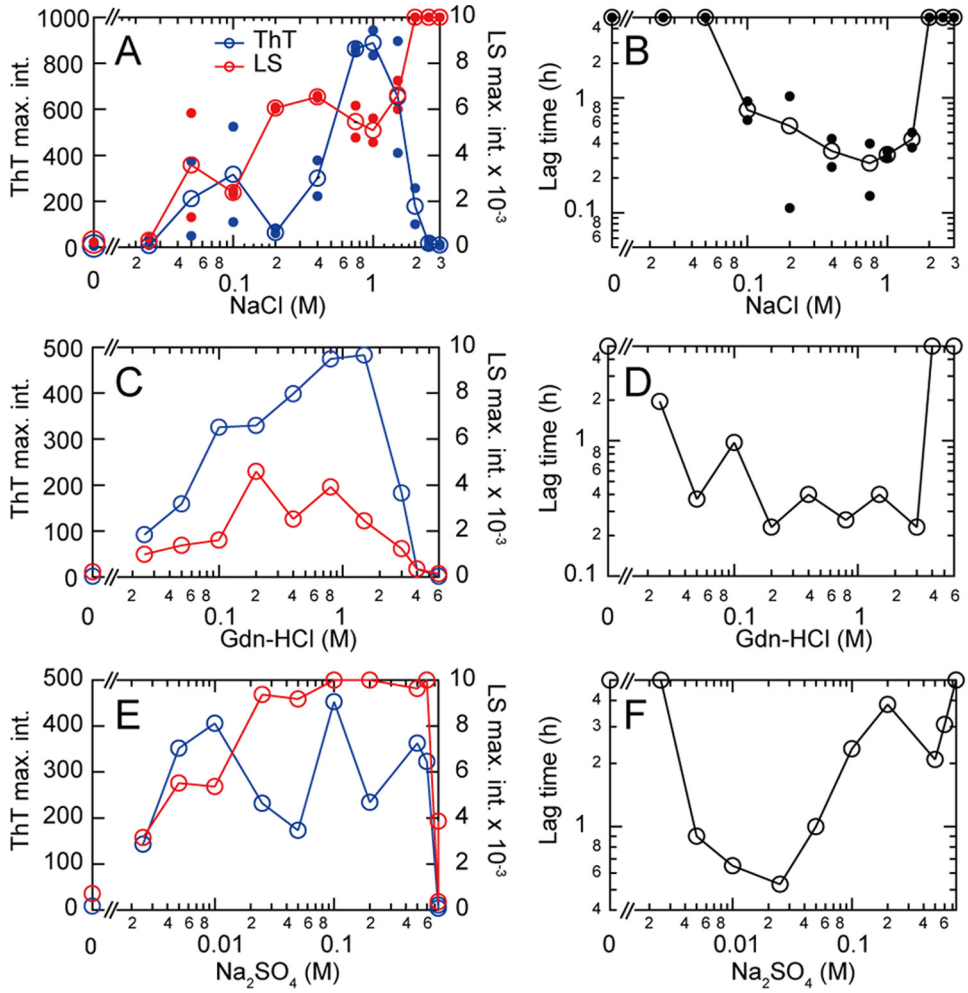

Figure 5. Effects of various salts on ultrasonication-dependent fibrillation of HEWL in 10 mM HCl at 60 °C. *A–F*, the effects of NaCl (*A* and *B*), Gdn-HCl (*C* and *D*), and Na_2SO_4 (*E* and *F*) were monitored under repetitive ultrasonic pulses of 4 min with 1-min quiescence. NaCl dependences of maximal ThT fluorescence at 485 nm and light scattering at 445 nm (*A*, *C*, and *E*) and lag time (*B*, *D*, and *F*) are plotted against salt concentration. Representative kinetics monitored by ThT fluorescence and light scattering are shown in Fig. S8.

Due to the fact that destabilization of the native structure is known to be an important requirement for fibrillation (30), we next studied the concentration-dependent effects of Gdn-HCl. Gdn-HCl induced fibrillation between 0.05 and 1.5 M with a maximum at around 1.0 M. Above 2.0 M, no fibrillation or amorphous aggregation was observed, with the solution remaining clear. At high concentrations, Gdn-HCl completely denatured HEWL thus preventing fibrillation. The effects of low concentrations of Gdn-HCl (*e.g.* 0.1 M) were similar to those of NaCl, suggesting that the effects of 0.1 M Gdn-HCl are because of anionic effects of chloride as seen for the Gdn-HCl-induced stabilization of the molten globule states (31).

Concentration-dependent effects of Na_2SO_4 were also studied to examine the hypothesis that sulfate groups might be specifically responsible for the promotion of fibrillation by heparin. Na_2SO_4 induced fibril formation at very low concentrations (*i.e.* around 2 mM) and was effective in facilitating fibrillation up to concentrations of 0.5 M. At 0.75 M, both fibrillation and amorphous aggregation appeared to be completely suppressed, suggesting stabilization of the native structure at these concentrations. Over the range of 0.02 to 0.05 M Na_2SO_4, ThT fluorescence was low and light scattering intensity was high, implying dominance of amorphous aggregates as for the cases of heparin and NaCl. The overall pattern for Na_2SO_4 resembled the general profile displayed by heparin. The results also showed that divalent sulfate anions at low concentrations (*i.e.* mM ranges) were more effective than their monovalent counterparts, possibly because of their capacity to form stronger electrostatic interactions with positively charged proteins (32). This finding is consistent with our previous results for β2m (33).

Direct photography of the turbidity and fluorescence of HEWL solutions in the presence of various concentrations of heparin, NaCl, Gdn-HCl, and Na_2SO_4 (with/without application of ultrasonic irradiation) provides a compact summary of the effects of varying ionic composition on the relative formation of fibrils and amorphous aggregates (Fig. 4 and Fig. S3). Consistent with the results monitored by fluorometer (Fig. 5 and Fig. S8), these photographs clearly depict the concentration-dependent and salt-type–dependent phase transitions of HEWL between (i) soluble states below the solubility limit or under supersaturation (clear wells by both light scattering and ThT fluorescence), (ii) a crystalline state (ThT-positive crystal-like fibrils), and (iii) a glassy state (ThT-negative but turbid amorphous aggregates).

Fibrillation in 50% (v/v) trifluoroethanol (TFE)

We previously reported amyloid formation from HEWL solutions containing TFE at pH 4.7 with applied ultrasonication (34). To further clarify the effects of heparin, we examined both heparin and simple salt-induced fibrillation of HEWL in 50% (v/v) TFE at 37 °C under ultrasonication (Fig. S9). Moreover, to further investigate the role of electrostatic attractions between negatively charged heparin and positively charged HEWL, we used gold nanoparticles coated with sulfate groups (Fig. S10). All of the results obtained in 50% TFE were consistent with those obtained in 10 mM HCl, confirming the role of electrostatic attractions between negatively charged heparin and positively charged HEWL (Fig. S2).

Discussion

Salt- and temperature-dependent conformation phase diagrams

Supersaturation is a solution condition where the apparent solute concentration is above the thermodynamic solubility and is a required condition to form crystals (8–10). Supersaturation may be caused by factors which block the normal transition mechanism, or alternatively those which encourage a competing pathway (35–37). The supersaturated state can often be "broken" by the addition of a ternary component which acts to circumvent the blocked kinetic transition from metastable to crystal form by offering a new pathway, possessing a lower energetic barrier. Simple examples of this phenomenon are provided by homogeneous seeding by crystal fragments and heterogeneous nucleation brought about by the intentional addition of impurities.

In this paper, we studied the effects of the ternary component heparin on HEWL fibrillation focusing on its role in regulating the partitioning of HEWL between crystal-like fibrils, glasslike amorphous aggregates, and soluble monomer. We have previously posited that, when the supersaturation condition is broken, quickly forming amorphous aggregation pathways are in competition with more slowly forming fibrillation pathways (14, 15). In such competitive situations, the slow breakdown and release of protein monomer from the amorphous aggregate is a prerequisite for its eventual incorporation into the amyloid fibrils. Our results showing the heparin-dependent competition of fibrillation and amorphous aggregation proved this basic hypothesis to be correct. On the other hand, the observed bimodal concentration dependence of heparin's enhancement of HEWL fibrillation (enhancement at low and high concentrations of heparin with inhibition at intermediate concentrations) was unexpected and is deserving of discussion.

To investigate the role(s) of heparin in facilitating the transition of HEWL between quaternary states, we constructed NaCl- or heparin-dependent effective phase diagrams at short and long times, respectively, corresponding to the supersaturation and thermodynamic equilibrium states (Fig. 6, *A* and *B*). We note that the phase diagrams before ultrasonication resemble those immediately after preparation of solutions. Comparison of the two phase diagrams shows that phase regions capable of supporting crystal-like HEWL amyloid fibrils were located near boundaries at the interface of soluble monomer and amorphous aggregation–rich regions. Supersaturated states were broken by application of ultrasonic irradiation. The most important finding is that there are two separate fibril-supporting phase regions at low and high heparin concentrations (Fig. 6*B*). The second region of fibrillation is defined by high concentrations of heparin above 10 mg/ml. This complicated two-stage pattern of heparin-dependent fibrillation has not been reported previously, including our previous study of the heparin-dependent fibrillation of β2m at low pH (27). The results suggest that there are two types of distinct mechanism of amyloid fibrillation (Fig. 7).

Anion binding-dependent fibrillation

In the absence of heparin, HEWL at low pH and high temperature (pH 2.0 and 60 °C) is largely denatured (HEWL T_m = 57 °C) and present as monomers (at least soon after the preparation of solutions) (Fig. 6 and Fig. S1). At low heparin concentrations, charge-charge attractions between the HEWL (pI = 11.3) and heparin lead to the generation of hetero-oligomeric networks of relatively large size (Fig. S5 and Table S1). There seems to be a certain concentration ratio of HEWL to heparin which promotes hetero-oligomerization and results in the formation of large extents of HEWL/heparin aggregate (Figs. 2, 4, and 6). We rationalize the existence of such a "sweet-spot" region (capable of promoting large hetero-oligomeric aggregates) as somewhat analogous to the case of immunoprecipitation reactions involving multivalent antigen and bivalent antibody complexes. In such immunoprecipitation reactions, specific ratios of reactant concentrations exist that are capable of generating either large percolated networks, or alternatively small aggregate species. In reference to the 0.25 mg/ml HEWL solution used in this study, for heparin concentrations below the μg/ml range, the relative concentration of HEWL to heparin is effectively saturating, thereby preventing extensive HEWL/heparin network formation, leading to a decrease in the size of the aggregate structures (Figs. S2, S5, and S6 and Table S1). At very high heparin concentrations, above 2 mg/ml the reverse case is true *i.e.* heparin saturates each HEWL, providing fewer chances to form large numbers of intermolecular crosslinks with other HEWL/heparin chains. In the intervening heparin concentration condition (~0.1–1 mg/ml) large percolation networks appear to be formed (Figs. S5 and S6 and Table S1) as evidenced by the intense light scattering signals measured over this region (Fig. 2).

Studies with various small anions indicated that the effects of heparin arise from sulfate groups on the basis of a mechanism similar to that observed for the anion-induced formation of acidic molten globule states of proteins (31, 32, 38–41). Those prior studies showed that multivalent anions are more effective than monovalent anions in inducing acidic molten globules. Anion effectiveness followed the electroselectivity series which represents the strength of direct charge-charge attractions (32) thereby making divalent sulfate more effective than monovalent chloride. Similar observations on anion electroselectivity were also found for the fibrillation of β2m under acidic conditions (33). As heparin possesses a large number of sulfate groups per molecule, it will likely exhibit stronger anionic effects through possession of a higher local charge density. In a

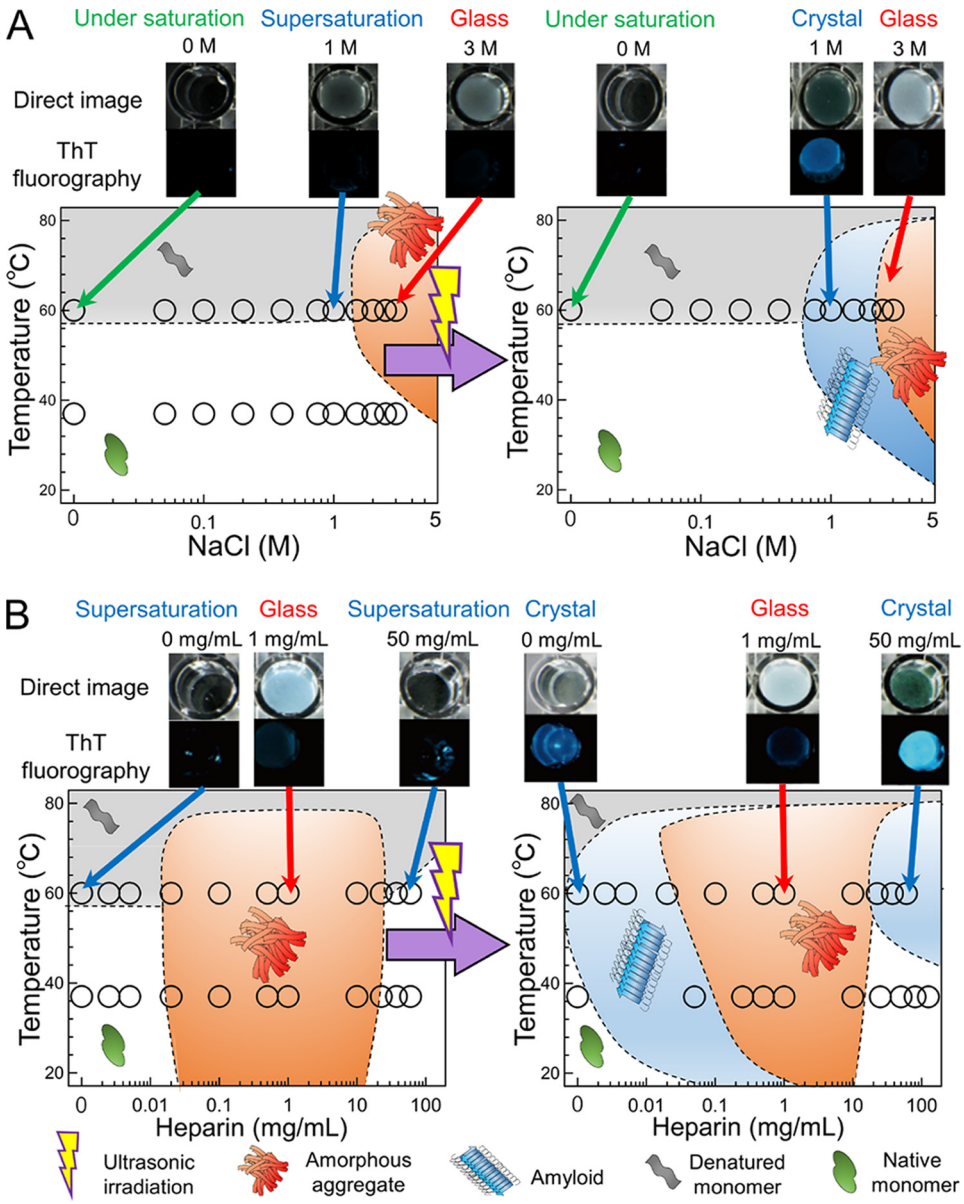

Figure 6. Conformational phase diagrams of HEWL dependent on supersaturation. *A*, temperature and NaCl concentration dependence. *B*, temperature and heparin concentration dependence. *Open circles* represent data points taken from Fig. 4 and representative well images are shown on the top of phase diagrams. Boundaries of different phases were drawn so as to fit the experimental data. Definitions of *cartoon symbols* are shown on the bottom of *panel B*.

likewise manner, the distribution of negative charges over the entire heparin polymer chain will make it multivalent with respect to binding the much smaller positively charged HEWL protein. In passing, we note that the effects of low concentrations of NaCl on stabilizing the molten globule state (31) were similar to those of Gdn-HCl, in which chloride also plays an obvious major role.

High heparin concentration–dependent fibrillation

A second stage of fibrillation, in which the lag time extended to several hours, was observed at very high heparin concentrations above 10 mg/ml (Fig. 2). Because of stabilization of HEWL by high concentrations of heparin (Fig. S1), the longer lag time may be because of frustration of the fibrillation process via a combination of increased stabilization of the native state and increased formation of HEWL/heparin hetero-oligomers. Based on the evidence, it seems likely that the driving force promoting the fibrillation of HEWL at high concentrations of heparin (Fig. 7) is a combination of general salting out effects (*i.e.* decreasing the solubility of proteins and peptides independent of their net charge (32, 42, 43)) and general excluded volume effects (produced by high concentrations of the large biopolymer heparin (44)) General salting out effects follow the Hofmeister series, relating to hydration of the generated ions (42, 43). Among the salts examined, the effects of Na_2SO_4 are the strongest, those of NaCl are slightly positive, and those of Gdn-HCl are negative (increased solubility of HEWL through induction of protein unfolding) (31, 32, 39, 40). Although macromolecular crowding effects tend to promote compact structure formation at increased heparin concentration (44), their consideration may resist simple interpretation as they would promote both oligomerization as well as protein-folding (44).

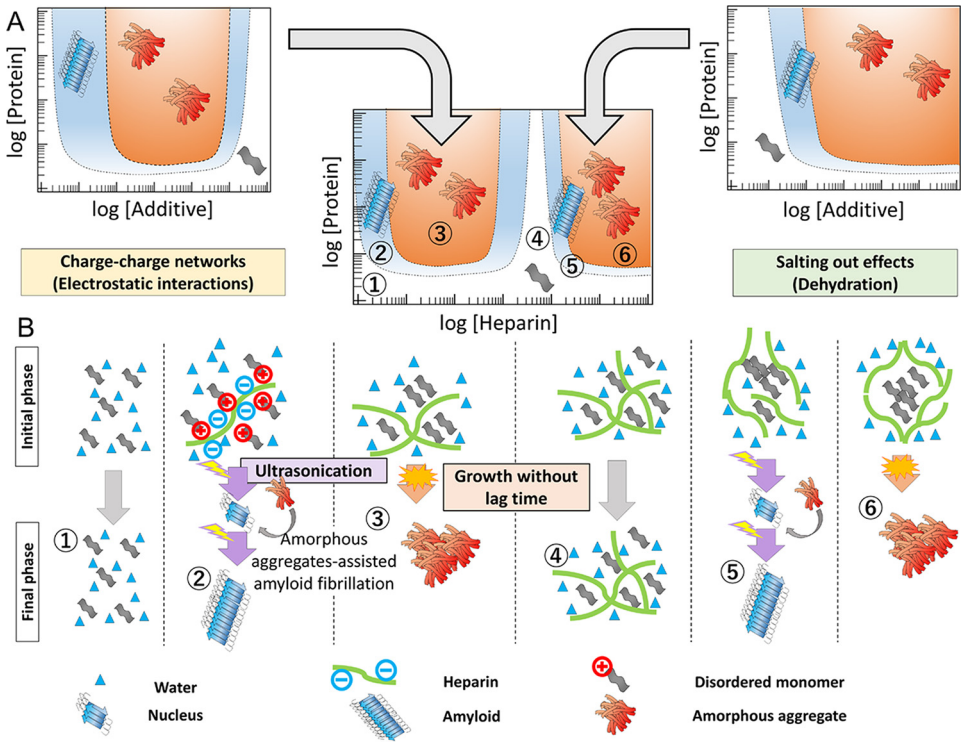

Figure 7. Mechanism explaining the heparin-dependent conformational phase diagram. Precipitation of HEWL was proposed to occur either by heparin-binding–induced charge-charge network formation or heparin-induced salting out/macromolecular crowding effects seen at high concentrations. Molecular models for the regions 1–6 of the complex phase diagram are illustrated below. The regions of crystal-like amyloid fibrils exist between the regions below saturation and those of glasslike amorphous aggregation. A small amount of amorphous aggregates formed under supersaturation were suggested to provide a site of heterogeneous nucleation.

Based on our findings, we speculate that the two-stage fibrillation may be operative for amyloidogenic proteins with positive net charge (*e.g.* β2m under acidic conditions). However, the first stage of fibrillation might be missing for amyloidogenic proteins without significant net charge (*e.g.* α-synuclein at neutral pH). With regard to this point, it has been previously reported that fibrillation of α-synuclein at neutral pH is dependent upon high concentrations of salt (45).

Roles of amorphous aggregates in determining rate of amyloid fibrillation

Competitive prevention of fibrillation—To date, amorphous aggregation and amyloid fibrillation have often been considered as separate pathways in direct competition with each other such that accumulation of amorphous aggregates will always retard fibrillation (8, 13, 14). In line with this view, amorphous aggregates formed at intermediate concentrations of heparin seem to completely prevent fibrillation over the time scale of observation (Fig. 2), as was previously observed for the salt-dependent fibrillation of β2m (14). The presence of two types of aggregates, which we describe as a frozen amorphous aggregation state and a labile amorphous aggregation state capable of slow fibrillation, are consistent with Ostwald's ripening rule of crystallization, in which morphologies of crystals change with time guided by their kinetic accessibilities and thermodynamic stabilities (9, 46). Importantly, in the Ostwald ripening mechanism, various pathways leading to distinct morphologies have been assumed to be independent and to compete with each other.

Amorphous aggregate–assisted fibrillation—For the conditions used in this study (100 mM NaCl, 10 mM HCl (pH 2.0), and 0.25 mg/ml HEWL), we observed that the acceleration of fibrillation at certain low concentration ranges of heparin was always accompanied by accumulation of a small amount of oligomeric aggregates, which cannot be explained by a competitive mechanism (Fig. 2). Although no pronounced aggregation was detected for different solution cases using NaCl, Gdn-HCl, or Na_2SO_4 (either in 10 mM HCl or 50% TFE at pH 4.8), it is likely that a small amount of aggregates or oligomers accumulate according to a competitive mechanism (14) and that these amorphous aggregates also play a role in unexpected acceleration of fibrillation. Experiments conducted investigating sulfate-coated gold nanoparticle-dependent fibrillation also suggested that sulfate-modified surfaces promote fibrillation through the formation of bound oligomeric complexes, although accumulation of such oligomers was not directly observed (Fig. S10). Taken together, these results suggest a novel mechanism of fibrillation in which spontaneous fibrillation is assisted by a small amount of glasslike amorphous aggregates/amorphous oligomers.

In crystallization studies, the rate of nucleation has been assumed to be proportional to the degree of supersaturation (10). A typical way of defining the degree of supersaturation (σ) is shown in Equation 1,

$$\sigma = \frac{\alpha - \alpha_0}{\alpha_0} \qquad \text{(Eq. 1)}$$

where α is the concentration of solute and α_0 is the critical concentration or thermodynamic solubility. We assume that amorphous aggregation is useful for increasing σ locally by increasing the concentration of amyloidogenic proteins in a manner similar to phase separation at the micro length scale. More specifically, amorphous aggregates increase the probability that a template-competent conformation emerges. Although their chance of formation may be very low, small amounts of template will be enough to break supersaturation of bulk protein solution, leading to explosive amyloid fibrillation via follow-on effects related to fragmentation of the growing fibrils (47, 48). We have previously speculated that such amorphous aggregation–assisted breakdown of supersaturation may occur at the surface of cavitation bubbles induced by the application of ultrasonic power (49).

We recall that supersaturation of solutes can be classified into two regions (10, 11). One is a "metastability" region, slightly above the solubility limit, where no spontaneous nucleation is assumed to happen and thus seeding is essential to break supersaturation. The other is a "labile" region, where spontaneous nucleation can happen after a lag time, leading to spontaneous crystallization. It is possible that the spontaneous nucleation in the labile regions is in fact triggered by the coexisting amorphous aggregates of solutes through heterogeneous nucleation (Fig. 7). Although heterogeneous fibrillation triggered by amorphous aggregates is similar to the secondary nucleation on seed fibrils, the seeding efficiency will be much less than that of real seeds because the chance for forming the seed-competent conformation is very low.

Amorphous aggregate–assisted acceleration of fibrillation has been suggested theoretically under conditions where oligomer formation is a rare event (50) and is highly consistent with a recent view of crystal nucleation involving a highly concentrated disordered droplet (35, 36, 51, 52). Most recently, Yamazaki *et al.* (53) used time-resolved liquid-cell TEM to perform an *in situ* examination of the nucleation of HEWL native crystals. Their TEM images revealed that amorphous solid particles act as heterogeneous nucleation sites. Their findings represent a significant departure from the existing formulation of the two-step nucleation and growth mechanism and suggest that amorphous particle– dependent heterogeneous nucleation is the dominant mechanism of spontaneous crystallization under supersaturation. Our results strongly suggest that a similar mechanism is important for amyloid fibrillation.

Conclusions

We showed that the heparin-induced amyloid fibrillation of HEWL was caused by either charge-charge attraction at low heparin concentrations or by general salting out effects at high heparin concentrations. Both mechanisms decrease the solubility of HEWL and thus induce insoluble aggregates, either crystal-like fibrils or glasslike amorphous aggregates. The importance of charge-charge interactions was confirmed by similar experiments in 50% TFE (Figs. S9 and S10), which also examined the effects of sulfate coated gold nano-particles on fibrillation. Heparin-assisted fibrillation always competed with amorphous aggregation. Such amorphous aggregate production may work positively or negatively for fibrillation, depending on their size, extent and stability. Extensive formation and stabilization of amorphous aggregates at intermediate heparin concentrations resulted in complete prevention of fibrillation. However, at lower heparin concentrations, conversion of rapidly formed amorphous aggregates to more stable fibrils occurs in accordance with Ostwald's ripening rule of crystallization (46).

Interestingly, a relatively small amount of such oligomeric and amorphous aggregates was likely to accelerate fibrillation. These findings suggest a novel role for amorphous aggregates in breaking supersaturation and thus triggering fibrillation, as was recently proposed for crystal nucleation facilitated by noncrystalline particles (53). Although we studied the interaction of negatively charged heparin and positively charged HEWL, amyloid fibrillation assisted by amorphous aggregates might be common to various accelerators where hydrophobic interactions or other attractive forces play roles in adsorbing monomers to form amorphous aggregates or oligomers. In this context, ultrasonication-dependent cavitation provides an effective nucleus factory for amyloid fibrillation (49).

Finally, visualization of the HEWL phase transition through comparison of ThT-fluorescence and light scattering (Fig. 4 and Fig. S3) emphasizes the similarity of fibrillation and crystallization of substances and indicates the importance of phase diagrams for understanding amyloid fibrillation. In future, direct quantification of the plate image will become a useful approach for characterizing the amyloid fibrillation and amorphous aggregation.

Experimental procedures

Materials

ThT was obtained from Wako Pure Chemical Industries, Ltd. (Osaka, Japan). HEWL, heparin with a molecular weight of ~13,000, and all other reagents were obtained from Nacalai Tesque (Kyoto, Japan).

Amyloid fibrillation

HEWL was dissolved in distilled water. The concentration of HEWL was determined spectrophotometrically at 280 nm with an extinction coefficient of 2.63 ml/mg/cm. Standard sample solutions contained 0.25 mg/ml HEWL, 5 μM ThT, 10 mM HCl (pH 2.0) and various concentrations of heparin, NaCl, Gdn-HCl, or Na_2SO_4. When HEWL fibrillation was monitored in 50% (v/v) TFE, 10 mM Na acetate buffer (pH 4.7) was used. A Hitachi fluorescence spectrophotometer F7000 or F4500 was used in which the sample solution in a cuvette with a 1-cm light path was irradiated with ultrasonic pulses from an ultrasonic generator tightly attached to a sidewall of the cuvette (Elekon Science Co., Chiba, Japan) (8). The solution was stirred with a stirring magnet at 600 rpm. Unless otherwise specified, ultrasonic conditions were cycles of 4-min ultrasonication and 1-min quiescence. The frequency and power of the ultrasonic pulses was 27.5 kHz and 0.14 watt, respectively. Fluorescence emission spectra from 440 to 560 nm were measured repeatedly with an excitation at 445 nm, and the 90° light scattering at 445 nm and ThT fluorescence at 485 nm were plotted (Fig. 1, *A* and *B*). Sample temperature was checked using a thermocouple (Compact Thermologger AM-8000K, Anritsu). Although we

used a water bath to keep the temperature of the sample solution, typically at 60 °C, the temperature increased up to a few degree during irradiation of the solution (14).

Direct photographic images of turbidity and ThT fluorescence were obtained under illumination of a microplate sample using either white light or blue LED light at 440 nm, respectively. For the 440-nm illumination, we used a handy LED lamp (Holkin, HLK-3AAA-1w, 430–440 nm) and the fluorescence image was observed through a 488-nm bandpass filter (Edmund Optics). Illumination was performed from four sides of the microplate and observation was done from the top of the plate.

TEM measurements

A sample solution (5 μl) was spotted onto a collodion-coated copper grid (Nisshin EM Co., Tokyo, Japan). After 1 min, the remaining solution was removed with filter paper and 5 μl of 2% (w/v) ammonium molybdate was spotted onto the grids. After 1 min, the remaining solution was removed in the same manner. TEM images were obtained with a Hitachi H-7650 transmission microscope (Tokyo, Japan) at 20 °C with a voltage of 80 kV and magnification of 15,000.

CD measurements

Using a 0.1 mg/ml HEWL solution, far-UV CD spectra (198–250 nm) were obtained with a Jasco spectropolarimeter J-720 or J-820 (Jasco Co., Ltd., Tokyo, Japan) using a quartz cell with a 1-mm path length at 37 °C. CD spectra were expressed in terms of mean residue ellipticity.

Author contributions—A. N., H. M., M. A., M. S., K. Sasahara, K. Sakurai, E. C., and K. N. performed experiments and analyzed data. H. O., D. H., and Y. G. designed experiments. The manuscript was written through contributions from all authors. All authors have given approval to the final version of the manuscript.

Acknowledgments—We thank Drs. Atsuo Tamura and Naoki Yamamoto (Kobe University) for valuable suggestions regarding dynamic light scattering measurement and data analysis and Takashi Naito (Institute for Protein Research) for performing some of experiments. D.H. acknowledges the receipt of a Senior Research Fellowship from the Australian National University and a Cross-Appointment Fellowship from the Institute for Protein Research.

References

1. Eisenberg, D., and Jucker, M. (2012) The amyloid state of proteins in human diseases. *Cell* **148,** 1188–1203
2. Tycko, R., and Wickner, R. B. (2013) Molecular structures of amyloid and prion fibrils: Consensus versus controversy. *Acc. Chem. Res.* **46,** 1487–1496
3. Sipe, J. D., Benson, M. D., Buxbaum, J. N., Ikeda, S., Merlini, G., Saraiva, M. J. M., and Westermark, P. (2014) Nomenclature 2014: Amyloid fibril proteins and clinical classification of the amyloidosis. *Amyloid* **21,** 221–224
4. Griffith, J. S. (1967) Self-replication and scrapie. *Nature* **215,** 1043–1044
5. Jarrett, J. T., and Lansbury, P. T., Jr. (1993) Seeding "one-dimensional crystallization" of amyloid: A pathogenic mechanism in Alzheimer's disease and scrapie? *Cell* **73,** 1055–1058
6. Lansbury, P. T., Jr., and Caughey, B. (1995) The chemistry of scrapie infection: implications of the 'ice 9' metaphor. *Chem. Biol.* **2,** 1–5
7. Wetzel, R. (2006) Kinetics and thermodynamics of amyloid fibril assembly. *Acc. Chem. Res.* **39,** 671–679
8. Yoshimura, Y., Lin, Y., Yagi, H., Lee, Y.-H., Kitayama, H., Sakurai, K., So, M., Ogi, H., Naiki, H., and Goto, Y. (2012) Distinguishing crystal-like amyloid fibrils and glass-like amorphous aggregates from their kinetics of formation. *Proc. Natl. Acad. Sci. U.S.A.* **109,** 14446–14451
9. So, M., Hall, D., and Goto, Y. (2016) Revisiting supersaturation as a factor determining amyloid fibrillation. *Curr. Opin. Struct. Biol.* **36,** 32–39
10. Bergfors, T. (2003) Seeds to crystals. *J. Struct. Biol.* **142,** 66–76
11. Crespo, R., Martins, P. M., Gales, L., Rocha, F., and Damas, A. M. (2010) Potential use of ultrasound to promote protein crystallization. *J. Appl. Crystallogr.* **43,** 1419–1425
12. Bemporad, F., and Chiti, F. (2012) Protein misfolded oligomers: Experimental approaches, mechanism of formation, and structure-toxicity relationships. *Chem. Biol.* **19,** 315–327
13. Miti, T., Mulaj, M., Schmit, J. D., and Muschol, M. (2015) Stable, metastable, and kinetically trapped amyloid aggregate phases. *Biomacromolecules* **16,** 326–335
14. Adachi, M., So, M., Sakurai, K., Kardos, J., and Goto, Y. (2015) Supersaturation-limited and unlimited phase transitions compete to produce the pathway complexity in amyloid fibrillation. *J. Biol. Chem.* **290,** 18134–18145
15. Hall, D., Kardos, J., Edskes, H., Carver, J. A., and Goto, Y. (2015) A multipathway perspective on protein aggregation: implications for control of the rate and extent of amyloid formation. *FEBS Lett.* **589,** 672–679
16. Cohlberg, J. A., Li, J., Uversky, V. N., and Fink, A. L. (2002) Heparin and other glycosaminoglycans stimulate the formation of amyloid fibrils from α-synuclein *in vitro*. *Biochemistry* **41,** 1502–1511
17. Yamamoto, S., Yamaguchi, I., Hasegawa, K., Tsutsumi, S., Goto, Y., Gejyo, F., and Naiki, H. (2004) Glycosaminoglycans enhance the trifluoroethanol-induced extension of β2-microglobulin-related amyloid fibrils at a neutral pH. *J. Am. Soc. Nephrol.* **15,** 126–133
18. Bazar, E., and Jelinek, R. (2010) Divergent heparin-induced fibrillation pathways of a prion amyloidogenic determinant. *ChemBioChem* **11,** 1997–2002
19. Bazar, E., Sheynis, T., Dorosz, J., and Jelinek, R. (2011) Heparin inhibits membrane interactions and lipid-induced fibrillation of a prion amyloidogenic determinant. *ChemBioChem* **12,** 761–767
20. Blancas-Mejía, L. M., Hammernik, J., Marin-Argany, M., and Ramirez-Alvarado, M. (2015) Differential effects on light chain amyloid formation depend on mutations and type of glycosaminoglycans. *J. Biol. Chem.* **290,** 4953–4965
21. Doig, A. J., and Derreumaux, P. (2015) Inhibition of protein aggregation and amyloid formation by small molecules. *Curr. Opin. Struct. Biol.* **30,** 50–56
22. So, M., Ishii, A., Hata, Y., Yagi, H., Naiki, H., and Goto, Y. (2015) Supersaturation-limited and unlimited phase spaces compete to produce maximal amyloid fibrillation near the critical micelle concentration of sodium dodecyl sulfate. *Langmuir* **31,** 9973–9982
23. Myers, S. L., Jones, S., Jahn, T. R., Morten, I. J., Tennent, G. A., Hewitt, E. W., and Radford, S. E. (2006) A systematic study of the effect of physiological factors on β2-microglobulin amyloid formation at neutral pH. *Biochemistry* **45,** 2311–2321
24. Bravo, R., Arimon, M., Valle-Delgado, J. J., García, R., Durany, N., Castel, S., Cruz, M., Ventura, S., and Fernàndez-Busquets, X. (2008) Sulfated polysaccharides promote the assembly of amyloid β(1–42) peptide into stable fibrils of reduced cytotoxicity. *J. Biol. Chem.* **283,** 32471–32483
25. Motamedi-Shad, N., Monsellier, E., Torrassa, S., Relini, A., and Chiti, F. (2009) Kinetic analysis of amyloid formation in the presence of heparan sulfate. *J. Biol. Chem.* **284,** 29921–29934
26. Noborn, F., O'Callaghan, P., Hermansson, E., Zhang, X., Ancsin, J. B., Damas, A. M., Dacklin, I., Presto, J., Johansson, J., Saraiva, M. J., Lundgren, E., Kisilevsky, R., Westermark, P., and Li, J. P. (2011) Heparan sulfate/heparin promotes transthyretin fibrillization through selective binding to a basic motif in the protein. *Proc. Natl. Acad. Sci. U.S.A.* **108,** 5584–5589
27. So, M., Hata, Y., Naiki, H., and Goto, Y. (2017) Heparin-induced amyloid fibrillation of β2-microglobulin explained by solubility and a

supersaturation-dependent conformational phase diagram. *Protein Sci.* **26,** 1024–1036
28. Hall, D., Zhao, R., Dehlsen, I., Bloomfield, N., Williams, S. R., Arisaka, F., Goto, Y., and Carver, J. A. (2016) Protein aggregate turbidity: Simulation of turbidity profiles for mixed-aggregation reactions. *Anal. Biochem.* **498,** 78–94
29. Zhao, R., So, M., Maat, H., Ray, N. J., Arisaka, F., Goto, Y., Carver, J. A., and Hall, D. (2016) Measurement of amyloid formation by turbidity assay-seeing through the cloud. *Biophys. Rev.* **8,** 445–471
30. Umemoto, A., Yagi, H., So, M., and Goto, Y. (2014) High-throughput analysis of the ultrasonication-forced amyloid fibrillation reveals the mechanism underlying the large fluctuation in the lag time. *J. Biol. Chem.* **289,** 27290–27299
31. Hagihara, Y., Aimoto, S., Fink, A. L., and Goto, Y. (1993) Guanidine hydrochloride-induced folding of proteins. *J. Mol. Biol.* **231,** 180–184
32. Goto, Y., Takahashi, N., and Fink, A. L. (1990) Mechanism of acid-induced folding of proteins. *Biochemistry* **29,** 3480–3488
33. Raman, B., Chatani, E., Kihara, M., Ban, T., Sakai, M., Hasegawa, K., Naiki, H., Rao C. M., and Goto, Y. (2005) Critical balance of electrostatic and hydrophobic interactions is required for β2-microglobulin amyloid fibril growth and stability. *Biochemistry* **44,** 1288–1299
34. Lin, Y., Lee, Y. H., Yoshimura, Y., Yagi, H., and Goto, Y. (2014) Solubility and supersaturation-dependent protein misfolding revealed by ultrasonication. *Langmuir* **30,** 1845–1854
35. Wallace, A. F., Hedges, L. O., Fernandez-Martinez, A., Raiteri, P., Gale, J. D., Waychunas, G. A., Whitelam, S., Banfield, J. F., and De Yoreo, J. J. (2013) Microscopic evidence for liquid-liquid separation in supersaturated $CaCO_3$ solutions. *Science* **341,** 885–889
36. Coquerel, G. (2014) Crystallization of molecular systems from solution: Phase diagrams, supersaturation and other basic concepts. *Chem. Soc. Rev.* **43,** 2286–2300
37. Matsushita, Y., Sekiguchi, H., Ichiyanagi, K., Ohta, N., Ikezaki, K., Goto, Y., and Sasaki, Y. C. (2015) Time-resolved X-ray tracking of expansion and compression dynamics in supersaturating ion-networks. *Sci. Rep.* **5,** 17647
38. Goto, Y., and Fink, A. L. (1989) Conformational states of β-lactamase: Molten-globule states at acidic and alkaline pH with high salt. *Biochemistry* **28,** 945–952
39. Goto, Y., Calciano, L. J., and Fink, A. L. (1990) Acid-induced folding of proteins. *Proc. Natl. Acad. Sci. U.S.A.* **87,** 573–577
40. Goto, Y., and Fink, A. L. (1990) Phase diagram for acidic conformational states of apomyoglobin. *J. Mol. Biol.* **214,** 803–805
41. Goto, Y., and Aimoto, S. (1991) Anion and pH-dependent conformational transition of an amphiphilic polypeptide. *J. Mol. Biol.* **218,** 387–396
42. Collins, K. D., and Washabaugh, M. W. (1985) The Hofmeister effect and the behavior of water at interfaces. *Q. Rev. Biophys.* **18,** 323–422
43. Washabaugh, M. W., and Collins, K. D. (1986) The systematic characterization by aqueous column chromatography of solutes which affect protein stability. *J. Biol. Chem.* **261,** 12477–12485
44. Hall, D., and Minton, A. P. (2003) Macromolecular crowding: qualitative and semiquantitative successes, quantitative challenges. *Biochim. Biophys. Acta* **1649,** 127–139
45. Yagi, H., Mizuno, A., So, M., Hirano, M., Adachi, M., Akazawa-Ogawa, Y., Hagihara, Y., Ikenoue, T., Lee, Y.-H., Kawata, Y., and Goto, Y. (2015) Ultrasonication-dependent formation and degradation of α-synuclein amyloid fibrils. *Biochim. Biophys. Acta* **1854,** 209–217
46. Levin, A., Mason, T. O., Adler-Abramovich, L., Buell, A. K., Meisl, G., Galvagnion, C., Bram, Y., Stratford, S. A., Dobson, C. M., Knowles, T. P., and Gazit, E. (2014) Ostwald's rule of stages governs structural transitions and morphology of dipeptide supramolecular polymers. *Nat. Commun.* **5,** 5219
47. Tanaka, M., Collins, S. R., Toyama, B. H., and Weissman, J. S. (2006) The physical basis of how prion conformations determine strain phenotypes. *Nature* **442,** 585–589
48. Hall, D., and Edskes, H. (2009) A model of amyloid's role in disease based on fibril fracture. *Biophys. Chem.* **145,** 17–28
49. Nakajima, K., Ogi, H., Adachi, K., Noi, K., Hirao, M., Yagi, H., and Goto, Y. (2016) Nucleus factory on cavitation bubble for amyloid β fibril. *Sci. Rep.* **6,** 22015
50. Auer, S., Dobson, C. M., and Vendruscolo, M. (2007) Characterization of the nucleation barriers for protein aggregation and amyloid formation. *HFSP J.* **1,** 137–146
51. Harano, K., Homma, T., Niimi, Y., Koshino, M., Suenaga, K., Leibler, L., and Nakamura, E. (2012) Heterogeneous nucleation of organic crystals mediated by single-molecule templates. *Nat. Mater.* **11,** 877–881
52. Vekilov, P. G. (2012) Crystal nucleation: Nucleus in a droplet. *Nat. Mater.* **11,** 838–840
53. Yamazaki, T., Kimura, Y., Vekilov, P. G., Furukawa, E., Shirai, M., Matsumoto, H., Van Driessche, A. E., and Tsukamoto, K. (2017) Two types of amorphous protein particles facilitate crystal nucleation. *Proc. Natl. Acad. Sci. U.S.A.* **114,** 2154–2159